A&A 490, 315–324 (2008)
DOI: 10.1051/0004-6361:200809957

Astronomy & Astrophysics

NLTE modelling of the flaring atmosphere above sunspot

A. Berlicki[1,2], P. Heinzel[3], B. Schmieder[1], and H. Li[4]

[1] Observatoire de Paris, Section de Meudon, LESIA, 92195 Meudon Principal Cedex, France
[2] Astronomical Institute, Wrocław University, 51-622 Wrocław, Poland
e-mail: berlicki@astro.uni.wroc.pl
[3] Astronomical Institute, Academy of Sciences of the Czech Republic, 25165 Ondřejov, Czech Republic
[4] Purple Mountain Observatory, Chinese Academy of Sciences, Nanjing 210008, PR China

Received 11 April 2008 / Accepted 9 July 2008

ABSTRACT

Aims. We performed an analysis of the solar flaring atmosphere above sunspots. During the flare on October 20, 2003 many flaring structures were observed projected onto the sunspots. We analysed the Hα and Ca II line profiles emitted by the ribbons partially overlapping the sunspots. In the penumbra, the line intensity in the far wings is lower than in a typical quiet Sun profile but the core emission of Hα and Ca II lines is typical for flares. We tried to find the structure of the flare observed above the sunspot penumbra using the observations of these chromospheric line profiles.
Methods. NLTE radiative transfer techniques allowed us to model the atmosphere of flaring structures and fit both the synthetic Hα and Ca II line profiles to the observed ones. We have derived semiempirical models of the flaring structure observed above sunspots.
Results. Our analysis shows that the flare emission observed within the sunspot penumbra comes from geometrically thin loop-like structures (cool flare loops) located above the fibrils of the penumbra. The structure of the penumbra located below the flare is almost not affected by the flare i.e. the flare emission in Hα and Ca II comes not from the upper chromosphere but from the structures that are higher in the corona. Therefore, a two-component modelling is necessary to reproduce the flare emission above the sunspot penumbra detected in our observations.

Key words. Sun: atmosphere – Sun: flares – sunspots – line: profiles

1. Introduction

Solar flares are commonly explained by magnetic field reconnections in the low corona. During the reconnection energetic particles (electrons and protons) are accelerated in the reconnection site. These particles propagate along the magnetic field lines down towards the chromosphere. As the plasma density is higher in these lower layers, the collisions of accelerated particles with the chromospheric plasma cause heating and lead to hard X-ray emission due to bremstrahhlung processes. Thus, bright ribbons are observed at both ends of hot flare loops. These ribbons are typically observed in chromospheric lines (e.g. Hα) and in EUV with SoHO, TRACE and Hinode. Moreover, the cool loops (misleadingly called "post-flare" loops (Švestka 2007)) are frequently seen connecting the flare ribbons. They may appear both in absorption or in emission, depending on the actual temperature and gas pressure (Heinzel & Karlicky 1987). These loops were extensively studied by many authors, see e.g. Heinzel et al. (1992); Schmieder et al. (1995, 1996).

Solar flares are almost always observed within or close to active regions (AR). The appearance of chromospheric emission of flares visible in the Hα line is determined by the configuration of the magnetic field in the active region. Sometimes, the bright emission of chromospheric plasma is observed very close to sunspots or even cospatial with sunspots. Such bright structures observed inside or above sunspots suggest that the plasma located above sunspots is heated by non-thermal electrons or by thermal conduction, as in non-sunspot flares.

Spectrophotometric analysis of chromospheric flare emission shows that enhanced emission is observed mainly close to the cores of chromospheric lines. For weak flares the emission in the line core is enhanced, but the Hα line may be still visible in absorption. For stronger flares the line becomes visible in emission, i.e. the intensity in line cores exceeds the intensity of neighbouring continuum (Machado et al. 1980). For weak and medium flares the continuum emission in the visible range is usually not disturbed. Only for very strong flares does the continuum emission of flaring kernels sometimes increase and we observe so called "white-light flares", which are visible outside strong chromospheric lines (Avrett et al. 1986; Mauas 1990; Mauas et al. 1990).

The majority of flares does not show enhanced continuum emission but only the chromospheric line emission. The level of visible continuum emission of the Sun is determined by the temperature of photospheric layers so this emission is formed below the chromosphere. The heating processes during solar flares are located mainly in the chromospheric layers. Therefore the radiation of chromospheric plasma changes significantly during solar flares and the intensity of all chromospheric lines is increased while the photospheric continuum emission is generally not affected. If the flare appears within or above the sunspot the heated chromosphere radiates strongly in the cores of chromospheric lines while the neighbouring continuum is lower than the quiet-Sun continuum due to the lower temperature inside sunspot umbra or penumbra (Li et al. 2005). The modelling of spectra emitted by sunspot umbra or penumbra was performed by several authors (Maltby et al. 1986; Ding & Fang 1989; Fontenla et al. 2006). This modelling as well as many spectral observations show that the intensity of the optical continuum emission of sunspots is significantly lower than the emission

from the quiet solar photosphere. However, there are no reports discussing the modelling of the sunspot atmosphere and its spectra affected by the flare.

The work that we present in this paper concerns the analysis of the Hα and Ca II emission of the flare located within the sunspot. We analysed the line profiles observed with the Multichannel Infrared Solar Spectrograph (MISS) at Purple Mountain Observatory (Li et al. 1999, 2002). Using the NLTE radiative transfer techniques (Heinzel 1995; Berlicki & Heinzel 2004; Berlicki et al. 2005) we modeled of the flare emission above the sunspots. These models allow us to analyse the structure of the flaring atmosphere together with the sunspot atmosphere below.

The paper is organized as follows. Section 2 presents the observations and a brief description of the active region and flare. In Sect. 3 we concentrate on the spectral data obtained with MISS spectrograph. In Sect. 4 we describe the NLTE radiative transfer methods used in our analysis and show our simulations of synthetic Hα line profiles obtained from NLTE codes. We also present the results of the modelling based on observational data. In Sect. 5 we discuss our results and present our conclusions concerning the validity of our modelling procedure and future prospects.

2. Observations of the solar flare on October 20, 2003

The 1N/M1.9 flare of October 20, 2003 was located at N03E48 and occurred in the active region NOAA 10484. The active region consists of one leading sunspot of positive polarity and several following sunspots of negative polarity. In the southern part of the region, penumbrae of positive polarity surround the negative sunspot group. With all these polarities the active region NOAA 10484 presents a δ configuration. This active region was observed by the THEMIS telescope on the Canary Islands in the MSDP (multichannel subtractive double pass) observing mode (Mein 2002). A detailed description of these observations can be found in Li et al. (2005). Figure 1 shows the longitudinal magnetograms obtained from the observations in the Na D1 line (upper panel) and the intensity image obtained in the chromospheric line Ca II 8542 Å.

The multi-channel infrared solar spectrograph (MISS) at Purple Mountain Observatory (PMO) (Li et al. 1999, 2002) observed this flare with the slit-pointing method. MISS observations started at 06:47 UT and ended at 07:58 UT, covering the impulsive and gradual phases of this flare. MISS observations consist of spectra in three lines – Hα, Ca II 8542 Å and He I 10830 Å – and Hα images obtained simultaneously with the spectra by the slit-jaw system of MISS, which uses a Daystar filter with 0.5 Å passband. The integration times of Hα, Ca II 8542 Å, and He I 10830 Å spectra are, respectively, 0.06 s, 0.06 s, and 0.4 s, while the spectral dispersions are 0.05453 Å, 0.05113 Å, and 0.04776 Å per pixel, respectively. The theoretical spatial resolution is 1.34″along the slit after 4-row binning, while the temporal resolution is about 2.8 s. The observed spectral data were first corrected for the dark-current, flat-field, scattered light and instrument profile, and then were calibrated absolutely using the continuum intensity near these wavelengths. The calibration was done by comparing the observed profiles emitted in the nearby quiet region with the reference mean profiles for Hα (David 1961) and Ca II 8542 Å (Linsky et al. 1970), and with an observed standard profile for He I 10830 Å (Li et al. 2005).

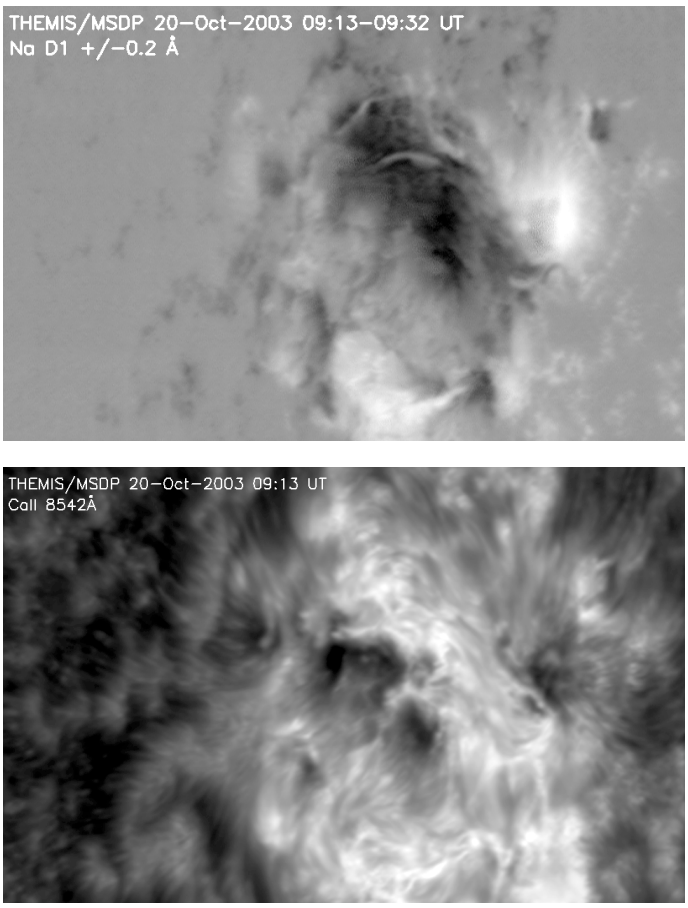

Fig. 1. THEMIS/MSDP longitudinal magnetic field of the AR 10484 observed on October 20, 2003 at 09:13–09:32 UT in the Na D_1 5896 Å line (*upper panel*) and the chromospheric emission observed in the Ca II 8542 Å (*lower panel*) line.

The 1N/M1.9 flare analysed in this paper was also observed by the RHESSI and SOHO/EIT instruments. In Fig. 2 we present the time evolution of the X-ray flux observed by GOES 10 during the flare.

3. Observed Hα and Ca II 8542 Å line profiles

In Fig. 3 we present nine slit-jaw images obtained by MISS in the Hα line. This sequence covers the impulsive and gradual phases of the flare. The coalignment of Hα images with magnetograms and intensity images of THEMIS and MDI shows that the ribbons are located over the magnetic neutral line and are cospatial with the penumbrae of the two sunspots separately (Fig. 4). In this image, we can clearly see two main Hα flare ribbons R1 and R2 and the slit of the MISS spectrograph crosses the brightest parts of the northern ribbon R1. This part of the Hα flare is located over the penumbra of the negative polarity sunspots.

In order to investigate the time evolution of chromospheric emission during the MISS observations, we selected spectra corresponding to the area in ribbon R1 marked by an arrow (Fig. 3). Theoretical spatial resolution of MISS slit-jaw images is 1.34″along the slit but the atmospheric seeing reduced it to about 2.5″. For each time of spectral observation we retrieved the profiles for all three observed lines (Hα, Ca II 8542 Å and He I 10830 Å). From these absolutely calibrated line profiles we computed the line-center intensities which are presented in Fig. 5 for Hα and Ca II (8542 Å) lines.

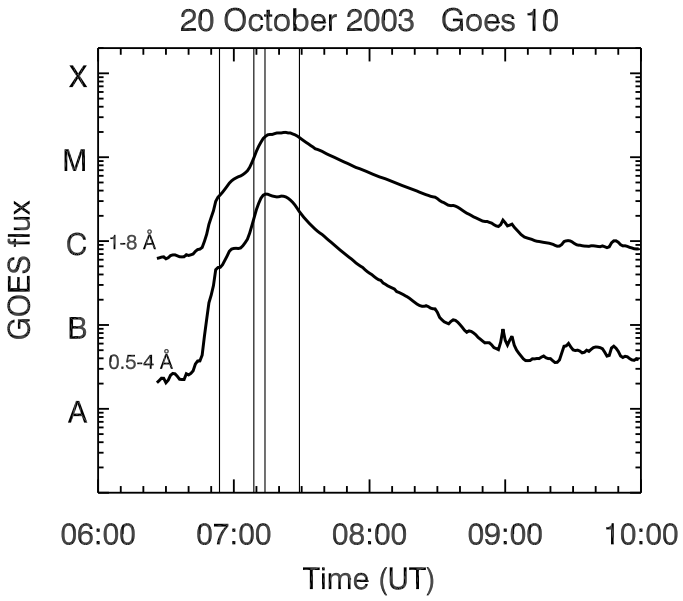

Fig. 2. GOES X-ray flux observed on October 20, 2003 during the flare. Black vertical lines denote the approximate times of the observed line profiles used in our detailed analysis.

The time behaviour of this emission is similar to the X-ray flux observed by GOES 10 during the flare. The time of maximum chromospheric emission is the same as the time of maximum soft X-ray emission. Li et al. (2005) showed that during the maximum of non-thermal hard X-ray emission the chromospheric line intensities exhibit a sudden increase which lasts a few minutes.

Among the many spectra obtained by MISS/PMO spectrograph we chose several ones to obtain the semiempirical models of the solar flaring atmosphere in the region indicated by the arrow in Fig. 3. Selected line profiles were observed at 06:53:40, 07:08:51, 07:13:47 and 07:29:01 UT and these times are indicated in Figs. 2 and 5. In our analysis we used Hα and Ca II 8542 Å lines. Observations of the He I 10830 Å line were not used because we do not calculate this line in our codes. Figure 6 presents an example of Hα and Ca II 8542 Å line profiles obtained for the analysed area at four times during the flare. These profiles exhibit emission in the line core which is typical for medium-size flares. As the flare developed, the line center emission increased and at the end of the analysed time sequence we observe a self–reversed profile. This kind of reversal is often observed in flares (Machado et al. 1980; Heinzel et al. 1994) but as we will see it can be explained in different ways (see e.g. Schmieder et al. 1987). At the same time, Ca II line profiles are in emission without self–reversal.

In the line profiles observed by the MISS spectrograph the intensity of the line wings (continuum) is lower than the corresponding intensity observed in quiet Sun areas (Fig. 6). This phenomenon appears because the analysed part of flare ribbons is located in projection within the sunspot penumbra. A detailed analysis of the structure of the atmosphere in these areas is given in the following sections.

4. Modelling of the flare chromosphere and the synthetic Hα and Ca II 8542 Å line profiles

We used the observed line profiles described in the previous section to construct models of the solar chromosphere corresponding to the analysed areas of the flare. In our analysis we concentrated on two lines (Hα and Ca II 8542 Å) in order to provide better modelling. These two lines are formed in the chromosphere but the height of the core and wings formation is different for each line. Therefore, by use of the two lines we can obtain a better sampling of parameters of the chromosphere. The codes which we use in the analysis were tested with these two lines simultaneously and we get a reasonable Hα and Ca II 8542 Å emission for each model of the atmosphere.

4.1. Semiempirical models of the flare chromosphere

The observed line profiles were compared with a grid of synthetic Hα and Ca II 8542 Å line profiles calculated with the NLTE codes developed by Heinzel (1995) and modified for flare conditions. Based on our experience in previous flare modelling, for our analysis we initially used "chromospheric" version of the codes. A detailed description of this method and codes is provided in Heinzel (1995); Berlicki & Heinzel (2004); Berlicki et al. (2005). We modified the codes used previously in the analysis of chromospheric flares and the previous input atmospheric model (VAL–C or F1) was currently replaced by the semiempirical model of sunspot penumbra obtained by Ding & Fang (1989). This atmospheric model is based on chromospheric lines observed at Kitt Peak Observatory and was constructed to describe the physical conditions in sunspot penumbra observed in July 3, 1985 close to the solar disk centre. The codes allowed us to find a model of the flaring chromosphere by varying input parameters: m_0 – modification of the column mass scale of the reference atmosphere, and ΔT which modifies the temperature distribution of the reference atmosphere (Berlicki & Heinzel 2004).

As mentioned above, as a starting model in our simulations we use the semiempirical model of sunspot penumbra developed by Ding & Fang (1989). In Fig. 7 (left panel) we present the height stratification of the temperature in this model compared to the other semiempirical models of the solar atmosphere: the VAL–C model of the quiet Sun (Vernazza et al. 1981), and FAL–S model of the sunspot umbra (Fontenla et al. 2006). The Ding & Fang model of the penumbra is characterised by a lower temperature compared to quiet Sun in the height range starting from the photospheric layers up to ≈1000 km above the photosphere. In the FAL–S model of the sunspot umbra the temperature is even lower in some layers of the atmosphere. These temperature distributions are responsible for the appearance of the Hα and other chromospheric line profiles for these models calculated with the NLTE codes (Hα in Fig. 7 – right panel). Both the intensities in the line core and line wings are lower than in the line from the quiet Sun (VAL–C). The continuum (line wing) emission is much weaker in a sunspot umbra or penumbra and this lowering depends on the depression of the temperature in the lower atmosphere of the Sun.

Using the grid of m_0 and ΔT parameters we reproduced the conditions in the flaring atmosphere in the sunspot penumbra, computed a set of models and reconstructed the corresponding Hα and Ca II 8542 Å line profiles for all chromosphere models. In order to account for a macroturbulent broadening of the line profiles we convolved all calculated profiles with a Gaussian function of half-width of around 0.25 Å (equivalent to 10 km s^{-1} at the Hα line wavelength). Then, we tried to find the best fit between synthetic and observed line profiles for all chosen times. We were able to obtain enhanced flare emission in both lines but unfortunately we could not obtain any agreement in the intensity

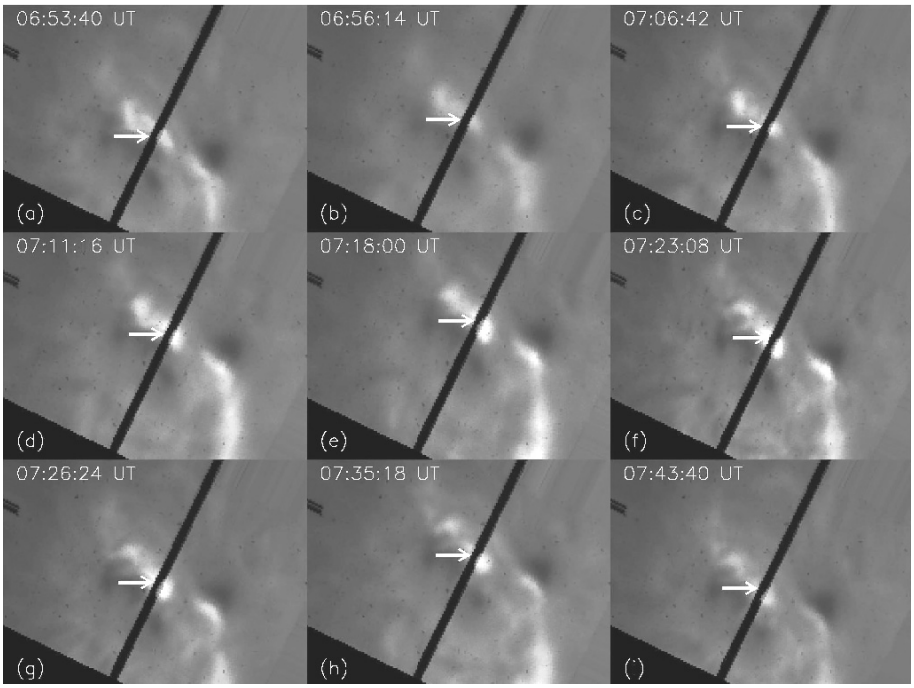

Fig. 3. Sequence of Hα slit-jaw images of the M1.9 flare on October 20, 2003. The arrow indicates the flare kernel used to obtain the Hα and Ca II line profiles.

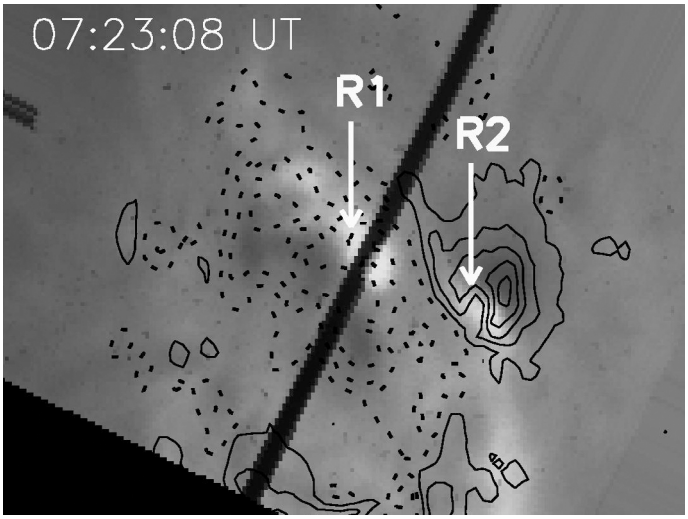

Fig. 4. Hα slit-jaw image with the contours of the longitudinal magnetic field observed by SOHO/MDI at 07:59:03 UT (solid line for positive and dotted line for negative polarity magnetic field). R1 and R2 mark the Hα flare ribbons.

for pairs of Hα and Ca II 8542 Å lines at any time. When we found a model where the Hα line profiles were well fitted, the calculated Ca II 8542 Å line profile exhibited a significant discrepancy from the observed one. And vice versa: for a model that gives good fitting of the Ca II 8542 Å line, we could not obtain an agreement between the synthetic and observed Hα line. We tried to change all input parameters of the model over a wide range but the result was always the same – impossible to fit both Hα and Ca II 8542 Å lines with the observations. One of the reasons could be that the model atmosphere we used is not realistic enough. In these calculations we assume that the flare emission is an integral part of the atmospheric model of a sunspot penumbra i.e. the flare volume is embedded in the penumbra atmosphere.

4.2. Two component models of the flaring structures above the sunspot penumbra

Hinode observations of a flare above sunspots give us another idea of how to construct models that could correctly reproduce both Hα and Ca II 8542 Å emission.

On December 13, 2006 the Solar Optical Telescope (SOT) on board the Hinode (Tsuneta et al. 2008) satellite observed an X3.4 flare in the Ca II H line. A detailed description of the flare itself and the observing details can be found in Isobe et al. (2007). On the movie covering the flare evolution we clearly see two ribbons which in a typical way separate from one another. The northern ribbon of this flare is much longer and its significant part is visible within the sunspot umbra and penumbra (Fig. 8). After detailed inspection of SOT images we noticed that the filamentary penumbral structures are overlayed by an arcade of flare loops which appear in emission. Within the penumbra, the flare emission consists of thin threads directed with a certain angle with respect to the penumbral structures. This observation leads us to the conclusion that the flaring structures are located higher than the sunspot penumbra. Thus, the flare emission comes from a "layer" located above the sunspot penumbra and consisting of portions of bright flaring loops. Note that such loops are frequently seen between flare ribbons. They are usually dark against the solar disk, but sometimes also in emission during initial phases of flares (e.g. Heinzel & Karlicky 1987; Heinzel et al. 1992). However, against the dark penumbra the loops can appear in emission.

Inspired by Hinode observations, for the analysed flare on October 20, 2003 we also assumed that the flaring plasma lies higher, forming a layer that is not related to the penumbra. Thus, we can perform a new two-component modelling of flare emission, where we independently simulate the emission of the penumbra by use of "chromospheric" NLTE codes and emission of flaring structures located above. For the latter we used the "filament" version of the NLTE codes (Heinzel et al. 1997). These codes were previously used to analyse filaments and arch filament systems (Schmieder et al. 1998; Mein et al. 2000, 2001) and, in general, they allow us to calculate the emission from cool

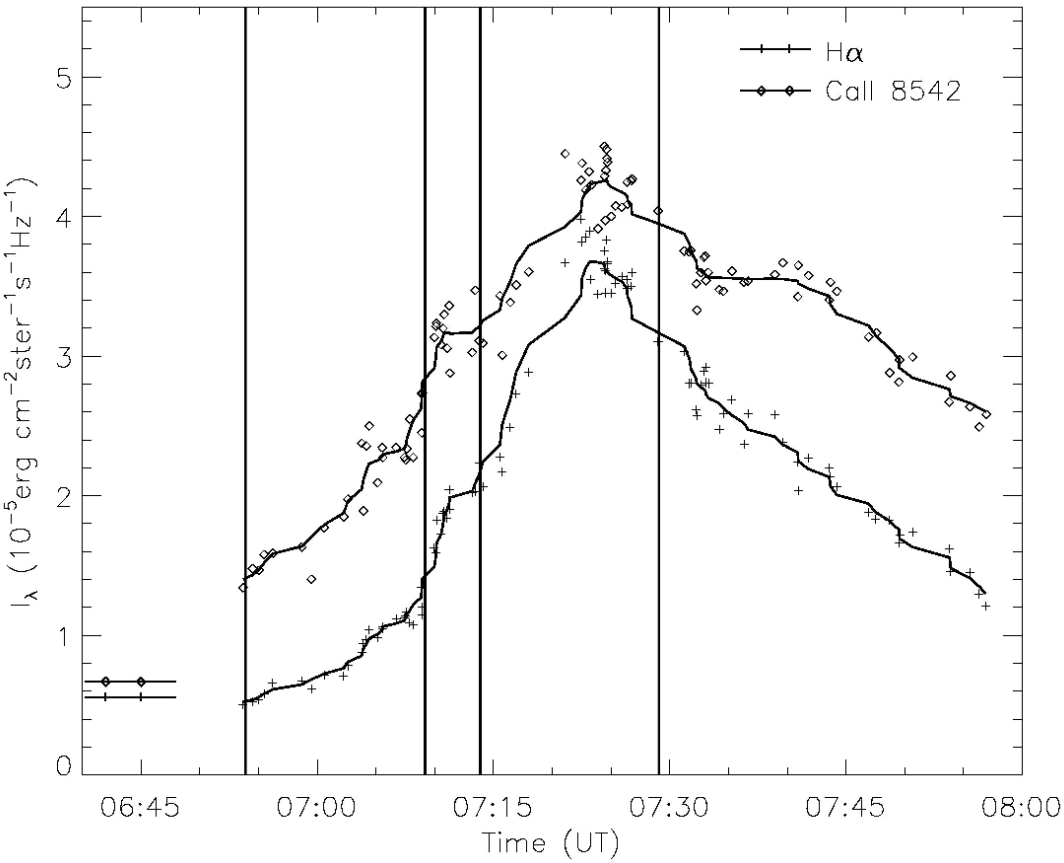

Fig. 5. Time evolution of the line-center intensities of Hα and Ca II 8542 Å lines observed by MISS at the point indicated by the arrow in Fig. 3. The symbols "+" and "⋄" correspond to the measured line-center intensities of Hα and Ca II 8542 Å and the solid lines are smoothed intensities. The horizontal short bars in the lower left side are corresponding line-center intensities observed in the nearby quiet Sun region. Black vertical lines denote the approximate times of the observed line profiles used in our detailed analysis.

isolated structures located in the corona. The main input parameters for these codes are the geometrical thickness of a horizontal slab (d), its temperature (T), gas pressure (p) and turbulent velocity ($V_{\rm turb}$). In this modelling the structure is isothermal and isobaric. By varying these parameters we can modify the intensity and shape of emergent spectral lines. A detailed description of these "filament" codes can be found in Heinzel et al. (1997).

The idea of this two-component modelling is the following. First, we modelled the penumbra atmosphere with the "chromospheric" codes. Then, using the "filament" version of the code we modelled a flaring layer above the penumbra. Next, we combined emission from the penumbra and from the flaring layer in order to obtain complete synthetic Hα and Ca II 8542 Å line profiles which should fit the observed spectra. The combination of these two emissions is expressed by the "cloud–model" formula (Mein & Mein 1988; Tziotziou 2007):

$$I(\lambda) = I_{\rm cloud}(\lambda) + I_{\rm pen}(\lambda)\, {\rm e}^{-\tau_{\rm cloud}(\lambda)}, \qquad (1)$$

where $I_{\rm cloud}(\lambda)$ is the intensity of cloud radiation computed by the "filament" code, $I_{\rm pen}(\lambda)$ is the intensity of the radiation emitted from the penumbra lying below, and $\tau_{\rm cloud}(\lambda)$ is the optical thickness of the cloud.

This formula allows us to obtain emergent intensity as a function of background and cloud intensities. In our case, the background corresponds to the emission of the sunspot penumbra obtained with "chromospheric" codes. The radiation of the cloud is calculated with "filament" codes and corresponds to a flaring layer. The optical thickness $\tau_{\rm cloud}(\lambda)$ comes from NLTE calculations.

The modelling of penumbra atmosphere was based on the best fit between the synthetic and observed wings of Hα and Ca II 8542 Å lines. In this way we constructed four models of the atmosphere in sunspot penumbra in the analysed area. These models do not contain the flare emission. In Fig. 9 we present results for the penumbra modelling. In the right panels the structure of the temperature is shown for four times of observation. In the temperature plots we did not notice any significant changes in the temperature distribution.

On the contrary, in the modelling of the flaring layer we fitted only the central parts of these lines, which contain the flare emission. For all times we obtained a set of parameters of the flaring layer and the emergent Hα and Ca II 8542 Å line profiles. During our initial calculations we noticed that for some models we were able to obtain self-reversed synthetic Hα line profiles but unfortunately the magnitude of central reversal was not in agreement with the observations. Calculated Hα line profiles exhibited stronger maxima and too low central minima. We removed this effect when we introduced a thin transition region zone between the cloud and surrounding corona. In our codes it is possible to define such a transition region as a layer of enhanced temperature at the top and bottom of our actual cloud. The enhancement of the temperature of the external parts of the cloud is due to the high temperature of the surrounding corona. Such transition regions were used previously in the modelling

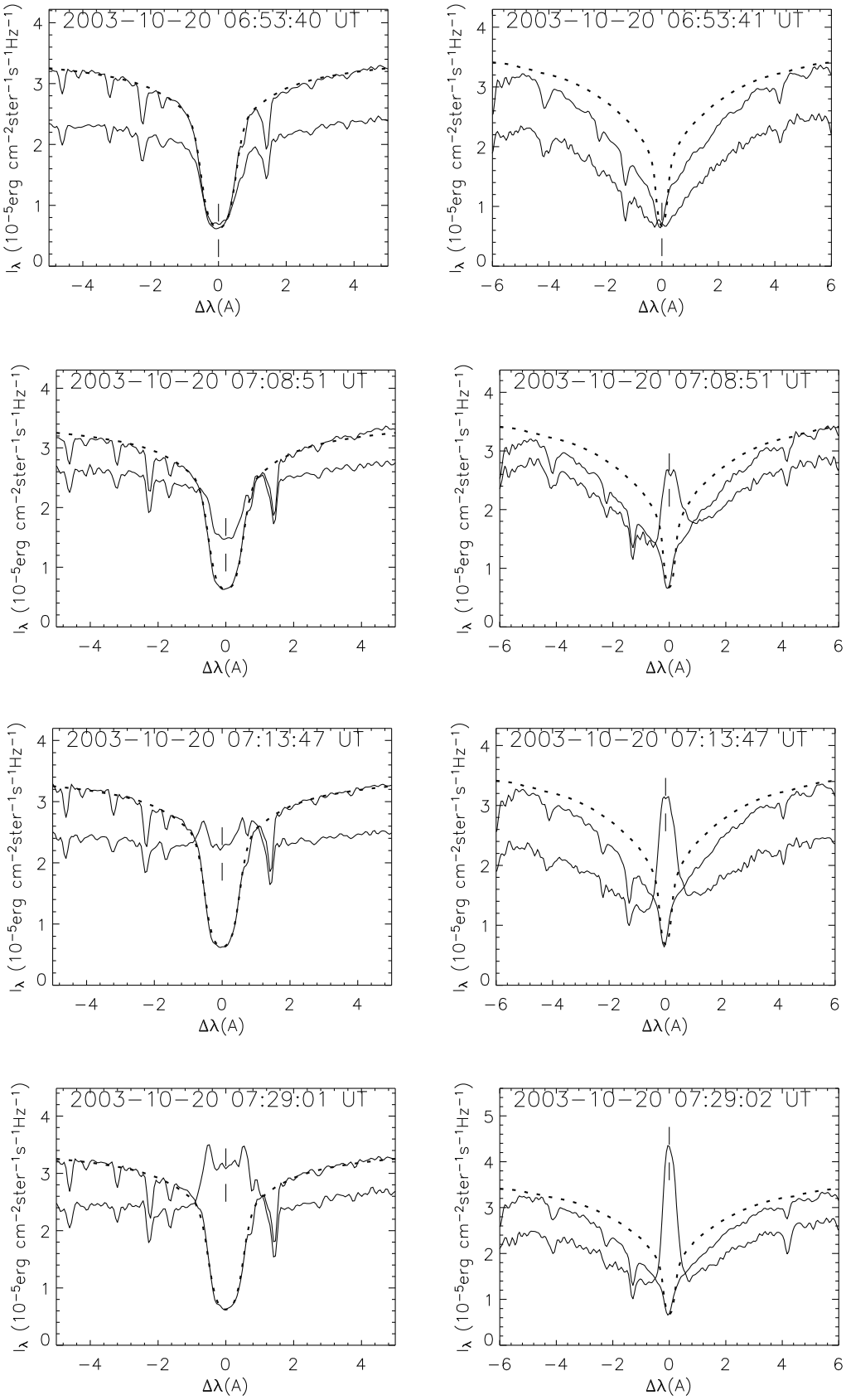

Fig. 6. Time evolution of Hα (*left column*) and Ca II 8542 Å (*right column*) line profiles observed simultaneously in a flare kernel located over a sunspot (see Fig. 3). Each panel shows two line profiles: flare emission (*lower solid lines*) and the mean quiet-Sun emission (*upper solid lines*) which is comparable to the reference profiles (dotted lines).

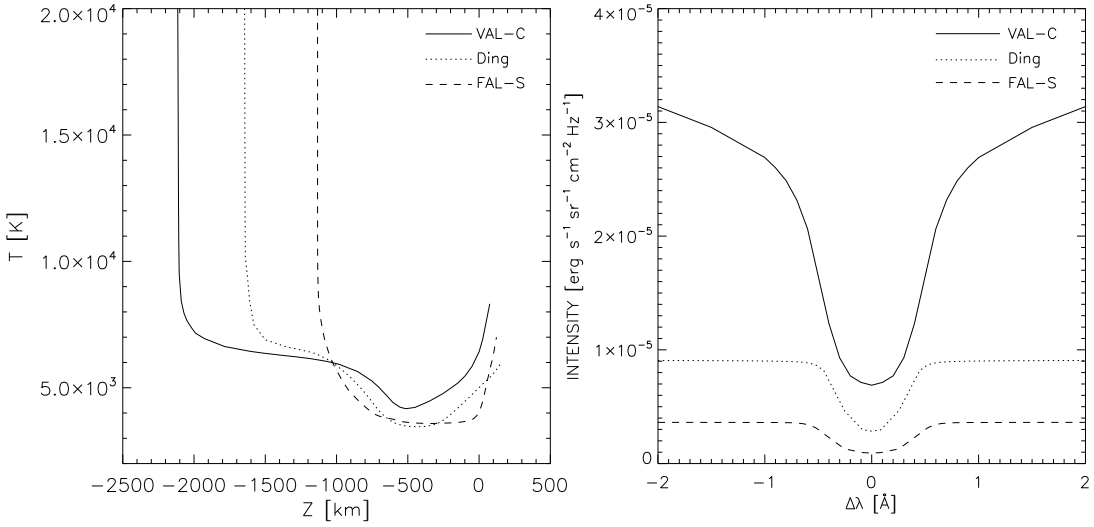

Fig. 7. Temperature as a function of height for three different models of the solar atmosphere: the VAL–C (solid line), Ding & Fang model of penumbra (dotted line), FAL–S model of sunspot umbra (dashed line). In the right panel we present corresponding synthetic Hα line profiles calculated for the appropriate models.

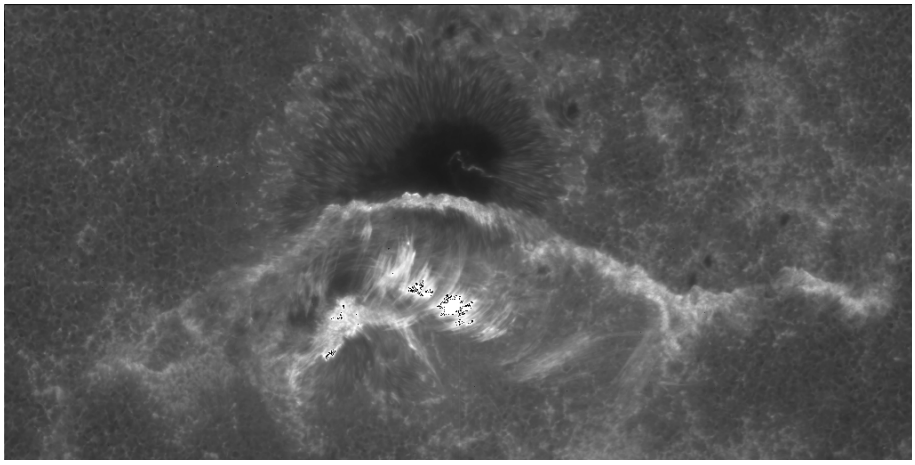

Fig. 8. Ca II H image of the flare on December 13, 2006 observed with Hinode/SOT. Note the penumbral structures visible through the bright flaring structures.

of filaments and prominences (Schmieder et al. 2003; Schwartz et al. 2006). In our case, the size of the central reversal of the Hα line became reliable when we introduced the transition region and we could obtain a good fit between observed and synthetic Hα and Ca II 8542 Å line profiles.

Figures 10 and 11 show synthetic line profiles emitted by the flaring layer. We also included the emission from the penumbra. In the top panels of these figures we plot line profiles emitted from the sunspot penumbra and from the cloud itself while in the lower panels we present the final fitting of the synthetic and observed line profiles. Synthetic line profiles were calculated with the "cloud–model" formula presented above. All synthetic profiles are convolved with a Gaussian function in order to reproduce the atmospheric and instrumental effects. Table 1 presents the parameters of the flaring layer obtained with the "filament" codes at four times of observation. In all four models we introduced a transition region of 0.3 km thickness and with a temperature of around 34 000 K outside the cloud.

The observed Hα and Ca II 8542 Å lines are now well fitted and their shapes are well reproduced. Even the self–reversal observed in the Hα line at the main phase of the flare is fitted quite well. In Figs. 10 and 11 we noticed that the differences between the observed and synthetic line profiles are not large. However, there are some differences within the central part of the Hα line. The calculated intensities of the central minimum and both peaks of this line differ somewhat from the observational data. The

Table 1. Parameters of the flaring cloud obtained using "filament" codes for the flare of October 20, 2003.

Time (UT)	d (km)	T (K)	p (dyn/cm^2)
06:53:40	170	7900	4.0
07:08:51	170	7600	19.0
07:13:47	180	7600	22.5
07:29:01	200	7950	27.0

instrumental effects and the Earth's atmosphere may influence the ratio between the intensities of the central minimum and the two peaks of the self-reversed Hα line profile. This ratio is then disturbed and the modelling may lead to less precise results. Also the width of the observed lines is influenced by the observational effects, which have to be taken into consideration (Berlicki et al. 2005).

The observed Hα and Ca II 8542 Å lines are rather symmetrical, but at 07:08:51 and 07:13:47 UT both line profiles exhibit a weak red asymmetry. In the Hα line we see a small redshifted component while Ca II is broadened towards longer wavelengths. Probably these features are due to a slow downflow of the flare plasma in the loops.

5. Discussion and conclusions

In this paper we studied the structure of the flaring atmosphere within the sunspot penumbra. For the first time the flare

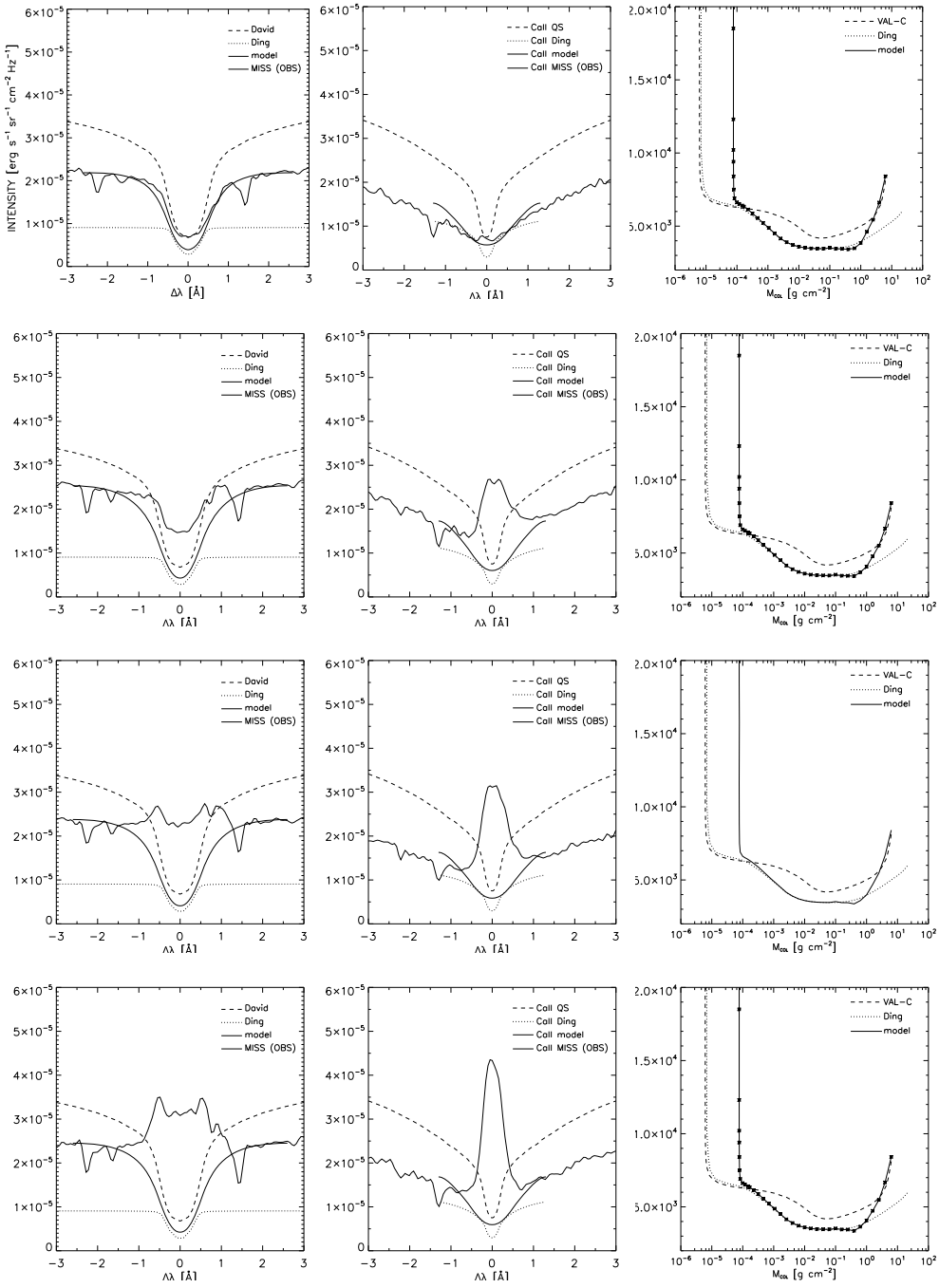

Fig. 9. Fitting of the line wings of the observed profiles by penumbra modelling with "chromospheric" codes (first component) plotted for all analysed times: 06:53:40 UT (first line), 07:08:51 UT (second line), 07:13:47 UT (third line) and 07:29:01 UT (fourth line). The first two columns show the Hα and Ca II 8542 Å lines. Thick solid lines represent the observed line profiles (MISS) while thin solid lines show the synthetic lines (model). The reference quiet Sun line profiles are plotted with dashed lines. The corresponding temperature structure of the penumbra is shown in the third column (solid lines with asterisks).

emission observed above a sunspot was studied quantitatively by using a NLTE radiative transfer modelling. In addition, simultaneous observations of two spectral lines, Hα and Ca II 8542 Å, were used for the modelling of the flare. To analyse the flare observed within the sunspot penumbra we used spectral observations from the MISS/PMO spectrograph of a flare on October 20, 2003. The flare occurred in NOAA 10484, which at that time was located relatively close to the solar disk centre, giving us the possibility of obtaining valuable Hα and Ca II 8542 Å line profiles of the flare emission above the penumbra used in the modelling of the atmosphere with the NLTE radiative transfer codes. These profiles were then used in the fitting procedure where we compared them with grids of synthetic profiles calculated with the NLTE codes. The fitting was performed by use of two different static codes: "chromospheric" and "filament". From the comparison of observed and synthetic profiles we found models of the solar chromosphere in the sunspot penumbra and models of the flaring layer (cloud) located above. In our analysis we chose one area observed at four different times during the flare.

The time behaviour of line-center intensities is similar to the thermal soft X-ray emission observed by GOES 10 which suggests that the flare emission observed in chromospheric lines is mainly due to the heating of the chromosphere by thermal conduction from the hot coronal parts of this flare. Here, the response of the chromosphere to the non-thermal heating is slow (Li et al. 2005, Fig. 10). The temporal evolution of the chromospheric line-center emission suggests that it could correspond to an accumulation of energy. This slow response of the chromosphere could be due to different phenomena, e.g. continuous heat flux from the hot corona or trapped particles. However, the

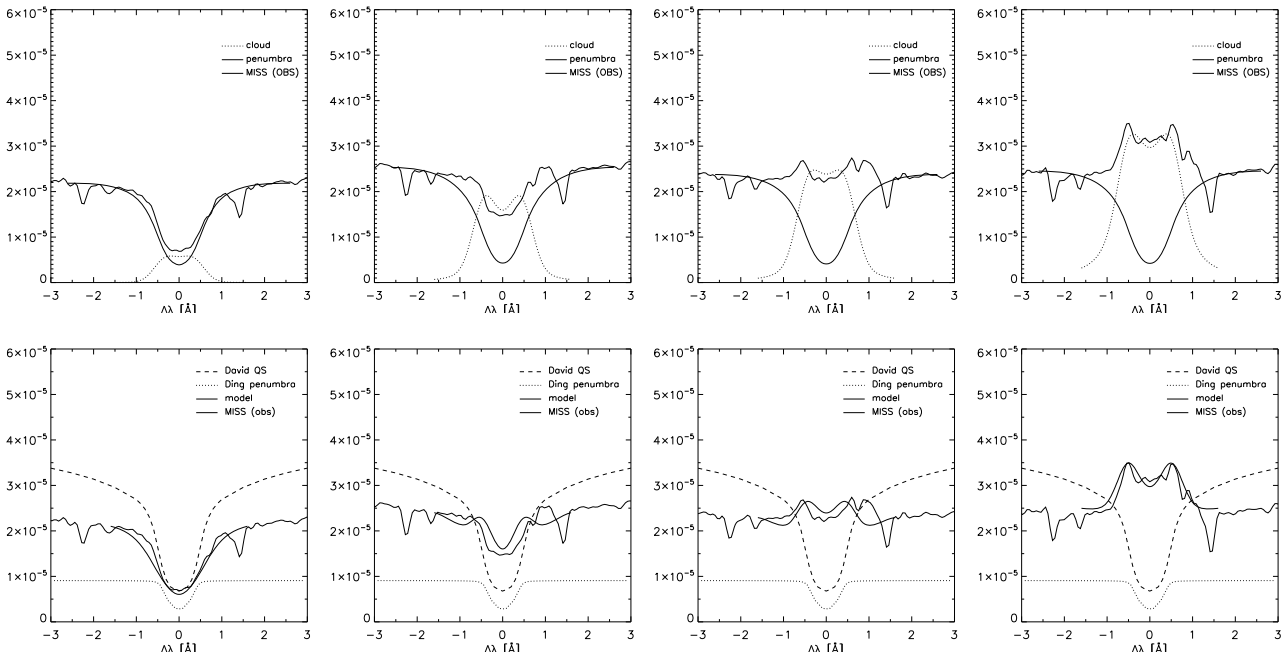

Fig. 10. Hα line: results of the both penumbra and flaring cloud model (first and second component) for all analysed times: 06:53:40, 07:08:51, 07:13:47 and 07:29:01 UT (four columns). Upper row: calculated Hα line profiles plotted separately for the sunspot penumbra (thin solid lines) and for the flare cloud (dotted lines). Observed line profiles are also shown for comparison (thick solid lines). Lower row: thick solid lines represent the resulting Hα line profiles calculated with formula (1), thin solid lines present the observations. Hα reference line profiles of the quiet Sun and the Ding & Fang model of penumbra are also shown.

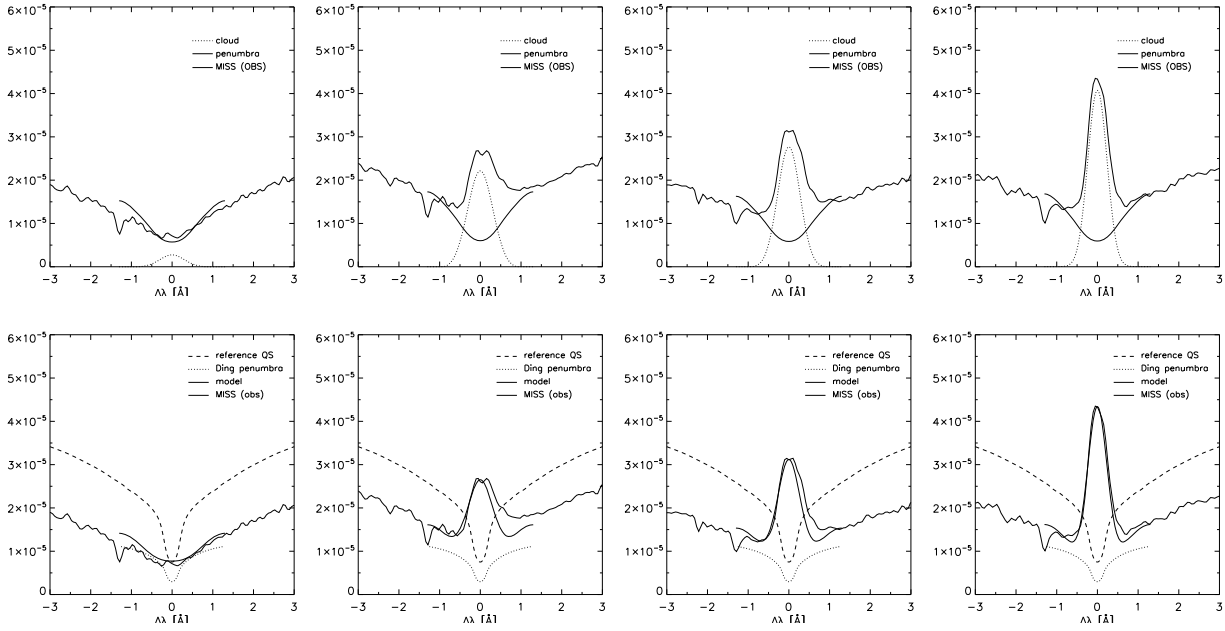

Fig. 11. Ca II 8542 Å line: results of the both penumbra and flaring cloud modelling (first and second component) for all analysed times: 06:53:40, 07:08:51, 07:13:47 and 07:29:01 UT (four columns). Upper row: calculated Ca II line profiles plotted separetely for the sunspot penumbra (thin solid lines) and for the flare cloud (dotted lines). Observed lines are also shown for comparison (thick solid lines). Lower row: Ca II 8542 Å line profiles calculated with formula (1) (thick solid lines), thin solid lines present the observations. Ca II reference line profiles of the quiet Sun and sunspot penumbra are also shown for comparison.

spectral analysis of X-ray emission performed by Li et al. (2005) suggests that thermal conduction is a dominant heating mechanism during this flare. Therefore we could obtain NLTE models of the chromosphere and the cloud without including the effects of non-thermal processes.

An inspection of Hinode/SOT observations of the flare on December 13, 2006 gave us an idea that the flare emission observed in projection above the sunspot penumbra is located higher than the penumbral structures. Therefore, we tried to construct a two-component model of the whole penumbra-flare

structure where we independently computed a model of a sunspot penumbra and a model of a flaring layer. Our calculations provided us with the structure of sunspot penumbra in the analysed area at four times. They showed that during the flare the model of the penumbra did not exhibit significant changes. The vertical structure of temperature and other parameters was almost constant during the whole period. This is consistent with the observations of the Hα and Ca II 8542 Å lines which exhibit a similar shape of their far line-wings. This suggests that the lower chromosphere and photosphere in the sunspot penumbra were not affected during this flare. This conclusion is based on the calculation of the contribution function of the Hα line, which describes the formation height of the different parts of the line profile (Kašparová & Heinzel 2002). The emission observed in the far wings of chromospheric lines comes from the very low chromosphere or photosphere. This emission did not change during the flare, which suggests that the heating mechanisms present in this flare had no significant effect on the lower layers of the atmosphere of the penumbra.

In the case of a flaring layer the situation is different. The modelling of this region showed that this layer is geometrically very thin. At 06:53:40 UT the obtained thickness of the flaring layer was ~170 km and it slightly increased to ~200 km as the flare developed. For all analysed times the temperature of the flaring layer also did not exhibit significant changes and it was always ~8000 K. The most evolving parameter of the flaring cloud was the gas pressure which increased from 4 dyn/cm^2 at the early phase of the flare to 27 dyn/cm^2 at 07:29:01 UT. This increase could be explained in the context of an evaporative model of the flare (Antiochos & Sturrock 1978). The amount of plasma in the flaring layers (loops) increased with time due to the evaporation of the chromosphere probably caused by the conductive heating from the reconnection site. Based on the experience obtained during the modelling process we conclude that the geometrical thickness and gas pressure had the most significant influence on the emission of the flaring layers. When we increase the thickness of the flaring layer while keeping the pressure constant (or the opposite) we obtained a higher emission in Hα and Ca II 8542 Å lines. However, the behaviour of the shape of the line profiles and the self–reversal of the Hα line allows us to distinguish between the effects of enhanced thickness and enhanced pressure. In the analysed flare only changes of gas pressure were significant for the reversal. We also noticed that the changes of the temperature of the flaring cloud has an important influence on the ratio between the Hα and Ca II 8542 Å line intensities. Therefore, this effect was used here for determination of the cloud temperature.

In our analysis we also found that self reversal of the Hα line profile may be a good proxy of the transition region located at the outer parts of cooler flaring cloud. Our analysis showed that this transition region is necessary to correctly reproduce the Hα line and the ratio of Hα and Ca II 8542 Å line center intensities also depends on the parameters of this transition region.

Observations of the flare on December 13, 2006 obtained by Hinode/SOT showed that the orientation of sunspot penumbral fibrils is different from the orientation of the threads (loops) that form the flaring layer. Such an orientation may be explained in the context of cool flare loops often observed in large flares (Heinzel et al. 1992; Schmieder et al. 1995, 1996). Probably, in the analysed flare the plasma is located in the more vertical magnetic field which forms cool flare loops. In the lower parts of these loops we observed bright flare threads located above the more horizontal penumbral fibrils. However, this aspect has to be investigated in detail. Our hypothesis is based only on the Hinode observations of another flare because the spatial resolution of the observations of October 20, 2003 is rather low.

To perform a more complete NLTE modelling and to confirm our two-component model of the flare above the sunspot penumbra it would be necessary to use spectroscopic observations obtained with higher spatial resolution. However, the models that uses observations of "cool" chromospheris lines (e.g. Hα or Ca II 8542 Å) concern only the coolest parts of the flare. The flare loops that we suggest as the model of our flare are probably loops at different temperatures, with hotter loops above the cooler ones. In this scenario, one particular loop has practically one temperature. The loops below 10 000 K will appear in Hα and Ca II 8542 Å; hotter (higher) loops may appear in the He I 10830 Å line which is formed at 10 000–20 000 K. Nevertheless, our current model will be unchanged.

Acknowledgements. The work of A.B. was supported by the Polish Ministry of Science and Higher Education, grant No. N203 016 32/2287. This work was also partly supported by ESA-PECS project No. 98030 and by the institutional project AV0Z10030501. The work of H.L. was supported by NSFC grants 10573038 and 10333040, the National Basic Research Program of China (2006CB806302), and the CAS Project KJCX2-YW-T04. We thank M. Siarkowski for providing the GOES 10 X–ray data. Hinode is a Japanese mission developed and launched by ISAS/JAXA, with NAOJ as domestic partner and NASA and STFC (UK) as international partners. It is operated by these agencies in co-operation with ESA and NSC (Norway).

References

Antiochos, S. K., & Sturrock, P. A. 1978, ApJ, 220, 1137
Avrett, E. H., Machado, M. E., & Kurucz, R. L. 1986, in The lower atmosphere of solar flares, 216
Berlicki, A., & Heinzel, P. 2004, A&A, 420, 319
Berlicki, A., Heinzel, P., Schmieder, B., Mein, P., & Mein, N. 2005, A&A, 430, 679
David, K.-H. 1961, Z. Astrophys., 53, 37
Ding, M. D., & Fang, C. 1989, A&A, 225, 204
Fontenla, J. M., Avrett, E., Thuillier, G., & Harder, J. 2006, ApJ, 639, 441
Heinzel, P. 1995, A&A, 299, 563
Heinzel, P., & Karlicky, M. 1987, Sol. Phys., 110, 343
Heinzel, P., Schmieder, B., & Mein, P. 1992, Sol. Phys., 139, 81
Heinzel, P., Karlicky, M., Kotrc, P., & Svestka, Z. 1994, Sol. Phys., 152, 393
Heinzel, P., Schmieder, B., & Vial, J.-C. 1997, in Fifth SOHO Workshop: The Corona and Solar Wind Near Minimum Activity, ed. A. Wilson, ESA SP, 404, 427
Isobe, H., Kubo, M., Minoshima, T., et al. 2007, PASJ, 59, 807
Kašparová, J., & Heinzel, P. 2002, A&A, 382, 688
Li, H., Fan, Z., & You, J. 1999, Sol. Phys., 185, 69
Li, H., You, J.-Q., Wu, Q.-D., & Yu, X.-F. 2002, Chinese Phys. Lett., 19, 742
Li, H., Berlicki, A., & Schmieder, B. 2005, A&A, 438, 325
Linsky, J. L., Teske, R. G., & Wilkinson, C. W. 1970, Sol. Phys., 11, 374
Machado, M. E., Avrett, E. H., Vernazza, J. E., & Noyes, R. W. 1980, ApJ, 242, 336
Maltby, P., Avrett, E. H., Carlsson, M., et al. 1986, ApJ, 306, 284
Mauas, P. J. D. 1990, ApJS, 74, 609
Mauas, P. J. D., Machado, M. E., & Avrett, E. H. 1990, ApJ, 360, 715
Mein, N., Schmieder, B., DeLuca, E. E., et al. 2001, ApJ, 556, 438
Mein, P. 2002, A&A, 381, 271
Mein, P. & Mein, N. 1988, A&A, 203, 162
Mein, P., Briand, C., Heinzel, P., & Mein, N. 2000, A&A, 355, 1146
Schmieder, B., Forbes, T. G., Malherbe, J. M., & Machado, M. E. 1987, ApJ, 317, 956
Schmieder, B., Heinzel, P., Wiik, J. E., et al. 1995, Sol. Phys., 156, 337
Schmieder, B., Heinzel, P., van Driel-Gesztelyi, L., & Lemen, J. R. 1996, Sol. Phys., 165, 303
Schmieder, B., Heinzel, P., Kucera, T., & Vial, J.-C. 1998, Sol. Phys., 181, 309
Schmieder, B., Tziotziou, K., & Heinzel, P. 2003, A&A, 401, 361
Schwartz, P., Heinzel, P., Schmieder, B., & Anzer, U. 2006, A&A, 459, 651
Tsuneta, S., Ichimoto, K., Katsukawa, Y., et al. 2008, Sol. Phys., 249, 167
Tziotziou, K. 2007, in The Physics of Chromospheric Plasmas, ed. P. Heinzel, I. Dorotovič, & R. J. Rutten, ASP Conf. Ser., 368, 217
Švestka, Z. 2007, Sol. Phys., 246, 393
Vernazza, J. E., Avrett, E. H., & Loeser, R. 1981, ApJS, 45, 635